

# An investigation on the leading and subleading high-energy behavior of hadron-hadron total cross sections using a best-fit analysis of hadronic scattering data

M. Giordano,<sup>1,\*</sup> E. Meggiolaro,<sup>2,†</sup> and P.V.R.G. Silva<sup>3,‡</sup>

<sup>1</sup>*Institute for Theoretical Physics, Eötvös University,  
and MTA-ELTE “Lendület” Lattice Gauge Theory Research Group,*

*Pázmány P. sétány 1/A, H-1117 Budapest, Hungary*

<sup>2</sup>*Dipartimento di Fisica dell’Università di Pisa, and INFN,  
Sezione di Pisa, Largo Pontecorvo 3, I-56127 Pisa, Italy*

<sup>3</sup>*Instituto de Física Gleb Wataghin,*

*Universidade Estadual de Campinas - UNICAMP, 13083-859 Campinas, SP, Brazil*

(Dated: September 23, 2018)

## Abstract

In the present investigation we study the leading and subleading high-energy behavior of hadron-hadron total cross sections using a best-fit analysis of hadronic scattering data. The parametrization used for the hadron-hadron total cross sections at high energy is inspired by recent results obtained by Giordano and Meggiolaro (2014) using a nonperturbative approach in the framework of QCD and it reads  $\sigma_{\text{tot}} \sim B \ln^2 s + C \ln s \ln \ln s$ . Both  $B$  and  $C$  are obtained by means of best-fits to data for proton-proton and antiproton-proton scattering, including recent data obtained at the LHC, and also to data for other meson-baryon and baryon-baryon scattering processes. The results are compared to the theoretical predictions existing in the literature. In particular, following the above-mentioned nonperturbative QCD approach, we also consider fits where the parameters  $B$  and  $C$  are set to  $B = \kappa B_{\text{th}}$  and  $C = \kappa C_{\text{th}}$ , where  $B_{\text{th}}$  and  $C_{\text{th}}$  are universal quantities related to the QCD stable spectrum, while  $\kappa$  (treated as an extra free parameter) is related to the asymptotic value of the ratio  $\sigma_{\text{el}}/\sigma_{\text{tot}}$ . Different possible scenarios are then considered and compared.

---

\* giordano@bodri.elte.hu

† enrico.meggiolaro@unipi.it

‡ precchia@ifi.unicamp.br

## I. INTRODUCTION

It is widely believed that the correct description of the strong interaction between quarks and gluons is provided by Quantum Chromodynamics (QCD), a belief supported by the numerous experimental verifications obtained in more than forty years. There are, however, energy regimes where the comparison between theory and experiment has not been performed yet, due to the lack of a theoretical prediction from the first principles of QCD. Such regimes are those where a major role is played by the nonperturbative dynamical aspects of QCD, which are notoriously very difficult to study. A successful comparison of experiment and theory in one of these regimes would certainly provide even stronger support to QCD being the appropriate description of strong interactions.

The total cross section ( $\sigma_{\text{tot}}$ ) for hadron-hadron scattering processes at high energy is one of the best known observables for which a fully satisfactory prediction from first principles is not yet available. The reasons why the theoretical study of this quantity in QCD is extremely difficult is better understood recalling the relation between  $\sigma_{\text{tot}}$  and the forward scattering amplitude provided by the optical theorem, which at high energy reads

$$\sigma_{\text{tot}}(s) \underset{s \rightarrow \infty}{=} \frac{\text{Im } F(s, t = 0)}{s}, \quad (1)$$

where  $s$  is the total center-of-mass energy squared and  $t = -\vec{q}^2$  is the transferred momentum squared. The optical theorem shows that the study of  $\sigma_{\text{tot}}$  requires the understanding of QCD in the regime of very low momentum transfer where the strong coupling constant becomes large [1], i.e., deep in the nonperturbative regime. On the other hand, at large  $s$  one cannot employ the main tool used in nonperturbative investigations of QCD, namely the lattice formulation of the theory, to compute directly the relevant quantities. The most interesting features of  $\sigma_{\text{tot}}$ , which should be explained by QCD, are its increase with energy at large energy, and the fact that the leading term is apparently universal, i.e., independent of the type of particles initiating the process.

More generally, the same limitations discussed above apply to the study of soft high-energy hadron-hadron scattering, i.e., scattering at large  $s$  and small  $|t| \lesssim 1 \text{ GeV}^2$ . Consequently, a full, model-independent description, obtained from the first principles of QCD, is not yet available for processes such as forward and near-forward elastic scattering. The study of soft high-energy physics has so far mostly proceeded through phenomenological models (for a recent review see Ref. [2]), on one side, and through general results obtained

using basic properties of the theory, like unitarity and analyticity. Such general results are usually incorporated in the phenomenological models, for example exploiting them to set constraints on the functional form of observables concerning their dependence on energy and momentum transfer. Regarding hadronic total cross sections, the most important such result is probably the Froissart-Lukaszuk-Martin (FLM) bound [3–5], which states that  $\sigma_{\text{tot}}$  cannot grow asymptotically faster than  $\ln^2 s$ , i.e.,

$$\sigma_{\text{tot}}(s) \leq B_{\text{FLM}} \ln^2(s/s_0) \quad (s \rightarrow \infty), \quad (2)$$

where  $\sqrt{s_0}$  is an undetermined energy scale, and the coefficient  $B_{\text{FLM}}$  is also bounded,

$$B_{\text{FLM}} \leq \frac{\pi}{m_\pi^2} \approx 60 \text{ mb}, \quad (3)$$

with  $m_\pi$  the  $\pi^0$  mass. The FLM bound and the theory of *Regge poles* (see, e.g., Refs. [6, 7]) are the inspiring principles behind the currently most successful phenomenological description of the experimental results for hadronic total cross sections (see below).

The recent measurements of  $\sigma_{\text{tot}}$  at the Large Hadron Collider (LHC) at CERN have brought back the attention to the energy dependence of this quantity at high energy, with several new phenomenological analyses of the data (see Ref. [2] and references therein). Such measurements, made by the TOTEM Collaboration at  $\sqrt{s} = 7$  TeV and  $\sqrt{s} = 8$  TeV [8–12], and by the ATLAS Collaboration at  $\sqrt{s} = 7$  TeV [13], are currently the highest-energy measurements performed at colliders. Recently there have also been some advancements on the theoretical side. Two of us have obtained the leading behavior of the total cross section for meson-meson scattering [14] in the framework of the nonperturbative approach to soft high-energy scattering in QCD proposed long ago by Nachtmann [15], and later developed by several authors [16–20]. In this approach the relevant scattering amplitudes are related to the correlation functions (in the sense of the functional integral) of certain Wilson loops, describing the classical trajectories of the colliding mesons. It has been argued that the same correlation functions should be relevant to the description of scattering processes involving baryons as well [17], so the results of Ref. [14] should apply to general hadronic processes. Under certain assumptions, the leading asymptotic energy dependence turns out to be of the “Froissart” type, i.e., proportional to  $\ln^2 s$ , with a universal prefactor, independent of the type of particles involved. More precisely, the first two leading terms in energy read

$$\sigma_{\text{tot}}^{ab}(s) \underset{s \rightarrow \infty}{\sim} B \ln^2 \left( \frac{s}{s_0^{ab}} \right) + C \ln \left( \frac{s}{s_0^{ab}} \right) \ln \left[ \ln \left( \frac{s}{s_0^{ab}} \right) \right], \quad (4)$$

where  $\sigma_{\text{tot}}^{ab}$  denotes the total cross section for the scattering of hadrons  $a$  and  $b$  with masses  $m_a$  and  $m_b$ , respectively, and  $s_0^{ab} = m_a m_b$ . The coefficients  $B$  and  $C$  are equal to  $\kappa B_{\text{th}}$  and  $\kappa C_{\text{th}}$ , respectively, where  $B_{\text{th}}$  and  $C_{\text{th}}$  are universal quantities related to the QCD stable spectrum, while the coefficient  $\kappa$  is, at the present stage, an undetermined real number with  $0 \leq \kappa \leq 2$ , connected to the asymptotic ratio between the total elastic cross section ( $\sigma_{\text{el}}$ ) and the total cross section as  $\sigma_{\text{el}}/\sigma_{\text{tot}} = \kappa/2$ . As experiments suggest universality of the  $\ln^2 s$  term, it is natural to *assume* that  $\kappa$  is universal as well. Making more detailed assumptions on  $\kappa$ , e.g., that a *black-disk* behavior is attained at high energy ( $\kappa = 1$ ), it is then possible to provide a *prediction* for the coefficient of the leading term in  $\sigma_{\text{tot}}$ , which turns out to be in fair agreement with the experimental results. Since a fair amount of assumptions is involved in the derivation, this result cannot be claimed to be “the” prediction of QCD. Nevertheless, to the best of our knowledge, this is the closest to a prediction that one has come so far.

We point out that a subleading term of the form  $\ln s \cdot \ln \ln s$  has appeared in other approaches to the study of  $\sigma_{\text{tot}}$ , namely (i) in a bound for the “energy-averaged” total cross section obtained by Martin and Roy [21], (ii) in a revision of Heisenberg’s model made by Nastase and Sonnenschein [22], where they assume that the Froissart bound is saturated, and (iii) in an improvement of the FLM bound in the AdS/CFT approach made by Díez *et al.* [23].

Regardless of its origin, the expression eq. (4) provides a perfectly good parametrization of the total cross section at high energy, that can be used to fit the experimental results, treating  $B$  and  $C$  as fitting parameters. It is then legitimate to investigate whether in this way one can improve over the currently most successful parametrizations, where this term is absent. In particular, given that new experimental information is now available at higher energies, one may ask whether the asymptotic subleading contribution in eq. (4) is already visible at LHC energies and, if so, how much this contribution is. The main purpose of the present analysis is precisely to test the functional form eq. (4), by means of fits to  $pp$  and  $\bar{p}p$  data, and by comprehensive fits to all the available data for meson-baryon and baryon-baryon scattering.

Besides this general purpose, our analysis allows to test the viability of the various approaches leading to an expression like eq. (4) for the total cross section. In particular, as already mentioned above, in the approach of Ref. [14]  $B$  and  $C$  are related to the QCD spectrum and to the elastic-to-total cross section ratio: this puts severe constraints on the

allowed values of  $B$  and  $C$ . In pursuing this line of investigation, the coefficients  $B$  and  $C$  can either be fixed to their theoretical prediction, or treated as free parameters when fitting the experimental data.

The paper is organized as follows. In section II we present a summary of some useful basic relations, and the results of Ref. [14] that constitute the basis of the present analysis. In section III we discuss the parametrization used in the fits and in section IV we detail the dataset considered. In section V we present and discuss the results obtained in the fits. Finally, we present our conclusions in section VI.

## II. SUMMARY OF THEORETICAL RESULTS

In this section we present a brief summary of the theoretical results of Ref. [14] concerning the asymptotic high-energy behavior of the elastic hadron-hadron scattering amplitude.

The approach employed in Ref. [14] is that originally proposed by Nachtmann [15] for elastic quark-quark scattering, and later expanded by several authors to describe hadron-hadron scattering [16–20]. In this approach, the elastic scattering amplitude in the soft high-energy regime ( $s \rightarrow \infty$ ,  $|t| \lesssim 1 \text{ GeV}^2$ ) of two mesons  $a$  and  $b$  with masses  $m_a$  and  $m_b$ , respectively, is obtained from the elastic scattering amplitude of two colorless dipoles of fixed transverse size, after folding with appropriate wave functions describing the colliding mesons. In turn, the dipole-dipole scattering amplitude is obtained from the (normalized, connected) correlation function of two Wilson loops in Minkowski space, running along the classical trajectories of the dipoles, in the limit of infinite longitudinal extension of the loops. Exploiting analytic continuation [24–30], it is possible to reconstruct these correlation functions from their Euclidean counterparts, which in turn can be related to the QCD spectrum by appropriately inserting a complete set of states between the two Wilson-loop operators. Under certain analyticity assumptions, discussed in detail in Ref. [14], it is then possible to derive the asymptotic behavior of the Minkowskian correlators at large energy and large impact parameter (which is the transverse distance between the classical trajectories of the incident particles), from which the elastic amplitude and the total cross section are finally obtained. The same chain of arguments can be used in the case of processes involving baryons, since similar Wilson-loop correlation functions are involved in the calculation of the corresponding scattering amplitudes [17], and the detailed transverse geometry of the

Wilson loops plays no role in the derivation of Ref. [14]. The results discussed below are therefore expected to be valid in more general hadronic processes than just meson-meson scattering. For more details, we invite the interested reader to confer the original references.

In Ref. [14] the elastic scattering amplitude was computed assuming that for asymptotically large energies one finds a *black-disk* behavior, corresponding to the Minkowskian Wilson-loop correlator tending to zero as the energy goes to infinity, for sufficiently large but fixed impact parameter. It is straightforward to generalize this result to the case where this correlator tends to a nonzero constant  $\kappa - 1$ , which we *assume* to be independent of the transverse size of the loops. Analyticity requires  $\kappa$  to be real, and unitarity then requires that  $\kappa \in [0, 2]$ . One then finds

$$F^{ab}(s, t) \underset{s \rightarrow \infty, t \rightarrow 0}{\sim} 4\pi i s \kappa \left( \frac{\eta}{\tilde{m}} \right)^2 \frac{J_1(x)}{x}, \quad (5)$$

if  $x \equiv \eta\sqrt{-t}/\tilde{m}$  is kept fixed. Here

$$\eta = \frac{1}{2} W(2e^{2(\tilde{s}-1)\chi}) = (\tilde{s} - 1)\chi - \frac{1}{2} \ln[(\tilde{s} - 1)\chi] + \frac{\ln[(\tilde{s} - 1)\chi]}{4(\tilde{s} - 1)\chi} + \dots, \quad (6)$$

with  $W$  the Lambert  $W$  function [31], and  $\chi = \ln(s/s_0^{ab})$  with  $s_0^{ab} = m_a m_b$ . In the equations above,  $\tilde{s}$  and  $\tilde{m}$  are, respectively, the spin and mass of the particle in the QCD stable spectrum that maximizes the ratio

$$l_p \equiv \frac{s_p - 1}{m_p} \quad (s_p > 1), \quad (7)$$

where  $s_p$  and  $m_p$  are the spin and the mass of particle  $p$ . By ‘‘QCD stable spectrum’’ we mean here all those particles that are stable when strong interactions are considered in isolation. The assumed independence of  $\kappa$  on the transverse size of the dipoles implies that the scattering amplitude eq. (5), obtained after trivially folding with the hadronic wave functions, is a universal function of  $x$ .

Taking the limit  $t \rightarrow 0$  in eq. (5) and using the optical theorem eq. (1), we get for the total cross section

$$\sigma_{\text{tot}}^{ab}(s) \rightarrow \frac{2\pi}{\tilde{m}^2} \kappa \eta^2 + \mathcal{O}(\eta). \quad (8)$$

Using now eq. (6), we obtain, up to first subleading order,

$$\sigma_{\text{tot}}^{ab}(s) \rightarrow \kappa \left\{ B_{\text{th}} \ln^2 \left( \frac{s}{s_0^{ab}} \right) + C_{\text{th}} \ln \left( \frac{s}{s_0^{ab}} \right) \ln \left[ \ln \left( \frac{s}{s_0^{ab}} \right) \right] \right\} + \mathcal{O}(\ln(s/s_0^{ab})), \quad (9)$$

with

$$B_{\text{th}} = 2\pi \frac{(\tilde{s} - 1)^2}{\tilde{m}^2}, \quad C_{\text{th}} = -2\pi \frac{(\tilde{s} - 1)}{\tilde{m}^2}. \quad (10)$$

Notice the relations

$$\frac{B_{\text{th}}}{C_{\text{th}}} = 1 - \tilde{s}, \quad 2\pi \frac{B_{\text{th}}}{C_{\text{th}}^2} = \tilde{m}^2. \quad (11)$$

We then find that in the limit  $s \rightarrow \infty$  both the leading and the subleading term in the total cross section are independent of the scattering particles.

We also want to mention that in Ref. [14] another subleading term of order  $\mathcal{O}(\ln s)$ , i.e.,  $Q^{ab} \ln(s/s_0^{ab})$ , was also found (and such a term is also present in the analysis of Ref. [23]). Contrary to the leading and subleading terms discussed above, the coefficient  $Q^{ab}$  is expected to depend on the colliding particles, even if our assumption on  $\kappa$  is met.

In Ref. [14] the values of  $B_{\text{th}}$  and  $C_{\text{th}}$  were estimated by maximizing the ratio eq. (7) over the higher-spin, QCD stable spectrum. The resulting ‘‘dominant’’ particle was found to be the  $\Omega^\pm$  baryon, with mass  $m_{\Omega^\pm} \approx 1.67$  GeV and spin 3/2, that yields [using eq. (10)]

$$B_{\text{th}}^\Omega = 0.22 \text{ mb}, \quad C_{\text{th}}^\Omega = -2B_{\text{th}}^\Omega = -0.44 \text{ mb}. \quad (12)$$

One of the assumptions in Nachtmann’s approach is that the processes of splitting and annihilation of partons inside hadrons can be neglected over a small time window around collision time [15]. The description of hadrons in terms of dipoles is therefore perhaps better justified in the *quenched* limit of the theory. In this case the relevant spectrum over which one has to maximize eq. (7) is the *glueball* spectrum of the pure-gauge theory. The states of interest here (for details see Ref. [14]) are the  $J^{PC} = 2^{++}$  glueball state, with mass  $m_{g2^{++}} \approx 2.40$  GeV, and the  $3^{+-}$ , with mass  $m_{g3^{+-}} \approx 3.55$  GeV, both calculated in the *quenched* approximation [32], for which one finds

$$B_{\text{th}}^{g2^{++}} = 0.42 \text{ mb}, \quad C_{\text{th}}^{g2^{++}} = -B_{\text{th}}^{g2^{++}} = -0.42 \text{ mb}, \quad (13)$$

and

$$B_{\text{th}}^{g3^{+-}} = 0.78 \text{ mb}, \quad C_{\text{th}}^{g3^{+-}} = -\frac{1}{2}B_{\text{th}}^{g3^{+-}} = -0.39 \text{ mb}. \quad (14)$$

The value of  $B_{\text{th}}$  obtained using the  $\Omega^\pm$  baryon is the closest to the values of  $B$  published in the Review of Particle Physics by the Particle Data Group (PDG). In the 2014 edition, fits to forward quantities using energies  $\sqrt{s} \geq 5$  GeV yielded  $B_{\text{PDG}} = 0.2704 \pm 0.0038$  mb [33]; in the 2016 edition the revised value is  $0.2720 \pm 0.0024$  mb, obtained from a fit to data with  $\sqrt{s} \geq 5$  GeV and including the most recent measurements at the LHC [34].

From the amplitude eq. (5) one can easily calculate the asymptotic behavior of the total elastic cross section  $\sigma_{\text{el}}^{ab}$  using

$$\sigma_{\text{el}}^{ab}(s) = \int_{-\infty}^0 dt \frac{d\sigma_{\text{el}}^{ab}}{dt}(s, t), \quad \frac{d\sigma_{\text{el}}^{ab}}{dt}(s, t) = \frac{1}{16\pi s^2} |F^{ab}(s, t)|^2, \quad (15)$$

and assuming that the small- $t$  region gives the dominant contribution. From this result and from eq. (9), we obtain

$$\frac{\sigma_{\text{el}}^{ab}}{\sigma_{\text{tot}}^{ab}} \sim \frac{\kappa}{2} \quad (s \rightarrow \infty). \quad (16)$$

Eqs. (5) and (16) show that, if  $\kappa < 1$  (i.e.,  $\sigma_{\text{el}}/\sigma_{\text{tot}} < 1/2$ ), the elastic scattering amplitude  $F^{ab}(s, t)$  behaves asymptotically as a *grey disk* with constant profile function equal to  $\kappa$  and radius growing as  $\ln s$ .<sup>1</sup> If  $\kappa = 1$  we have the so-called *black disk* ( $\sigma_{\text{el}}/\sigma_{\text{tot}} = 1/2$ ), and if  $\kappa > 1$  we have the *antishadowing* regime ( $\sigma_{\text{el}}/\sigma_{\text{tot}} > 1/2$ ) [36, 37].

We want to stress the fact that so far we have assumed that  $\kappa$  is a universal parameter. Although this assumption is made plausible by the observed universality of total cross sections at high energy, a more general analysis should start with a particle-dependent parameter,  $\kappa^{ab}$ , and universality should then emerge from the fit results rather than being imposed *a priori*. This would however increase considerably the number of fitting parameters. Therefore, even if this case is not the most general one, we will consider  $\kappa$  as a universal parameter in the present analysis.

### III. PARAMETRIZATION OF THE TOTAL CROSS SECTION

In this work we want to study the leading and subleading high-energy behavior of hadron-hadron total cross sections using a best-fit analysis of hadronic scattering data. The available data of highest energy (excluding cosmic rays) are those for  $pp$  scattering at 8 TeV at the LHC [12, 38, 39] and for  $\bar{p}p$  scattering at 1.8 TeV at the Tevatron. If we want to include also data from other meson-baryon and baryon-baryon scattering processes (which are available only for  $\sqrt{s} \lesssim 25$  GeV), we need a parametrization for the low-energy region as well. In this

<sup>1</sup> We remind the reader that if one expresses the elastic amplitude  $F(s, t)$  in terms of the *profile function*  $\Gamma(s, b)$ , i.e. (assuming azimuthal symmetry) [7, 35],  $F(s, t) = 4\pi i s \int_0^\infty db b J_0(b\sqrt{-t})\Gamma(s, b)$ , with  $b$  the absolute value of the impact parameter, then the so-called *grey disk* of radius  $R(s)$  is a simple model in which  $\Gamma_{\text{GD}}(s, b) = \Gamma_0(s)$  for  $0 \leq b \leq R(s)$ , and  $\Gamma_{\text{GD}}(s, b) = 0$  for  $b > R(s)$ , which leads to  $F_{\text{GD}}(s, t) = 4\pi i s R(s) \Gamma_0(s) J_1(R(s)\sqrt{-t})/\sqrt{-t}$  and, using eq. (15) and the optical theorem eq. (1), to  $\sigma_{\text{el}}/\sigma_{\text{tot}} = \Gamma_0(s)/2$ .

section we present our parametrization for the total cross section and we fix the notation for the best-fit variants considered in our analysis.

We will divide the total cross section in two parts, aimed at describing the low-energy (LE) and the high-energy (HE) regions, respectively:

$$\sigma_{\text{tot}}(s) = \sigma_{\text{LE}}(s) + \sigma_{\text{HE}}(s). \quad (17)$$

As usual in the literature, we parametrize the energy dependence of  $\sigma_{\text{tot}}(s)$  at low energy by means of *Reggeon* exchange in the  $t$ -channel [6, 7]. The Reggeon-exchange contribution reads

$$R_i^{ab}(s) = A_i^{ab} \left( \frac{s}{s_0^{ab}} \right)^{-b_i} \quad (i = 1, 2), \quad (18)$$

where  $A_i^{ab}$  is associated to the residue function and  $b_i$  to the intercept of the Reggeon trajectory  $\alpha_i(t)$ , i.e.,  $b_i = 1 - \alpha_i(0)$ . We consider two Reggeon contributions: the index  $i = 1$  corresponds to a trajectory with *even* signature, while  $i = 2$  corresponds to a trajectory with *odd* signature. The latter contributes with a *minus* sign to  $ab$  scattering and with a *plus* sign to the crossed channel,  $\bar{a}b$ . Summarizing, the low-energy parametrization reads<sup>2</sup>

$$\sigma_{\text{LE}}^{a\pm b}(s) = A_1^{ab} \left( \frac{s}{s_0^{ab}} \right)^{-b_1} \mp A_2^{ab} \left( \frac{s}{s_0^{ab}} \right)^{-b_2}. \quad (19)$$

The high-energy contribution is parametrized by adding to the leading ( $\sim \ln^2 s$ ) and sub-leading ( $\sim \ln s \cdot \ln \ln s$ ) terms also a constant term  $A_{\mathbb{P}}^{ab}$  (which is usually understood as the contribution of the *critical Pomeron*, i.e., a simple pole in the complex angular-momentum plane with intercept  $\alpha_{\mathbb{P}}(0) = 1$ );<sup>3</sup> i.e.:

$$\sigma_{\text{HE}}^{a\pm b}(s) = A_{\mathbb{P}}^{ab} + \kappa \left\{ B \ln^2 \left( \frac{s}{s_0^{ab}} \right) + C \ln \left( \frac{s}{s_0^{ab}} \right) \ln \left[ \ln \left( \frac{s}{s_0^{ab}} \right) \right] \right\}, \quad (20)$$

where, following the analysis of Ref. [14] (briefly recalled in sec. II),  $B$  and  $C$  are treated as *universal* parameters, while  $A_{\mathbb{P}}^{ab}$ , as well as  $A_1^{ab}$  and  $A_2^{ab}$ , are *reaction-dependent*. As already said at the end of sec. II, we shall also assume (as in Ref. [14]) that  $\kappa$  is independent of the properties of the scattering particles. We consider the energy scale to be a fixed parameter and to depend only on the masses of the scattering particles,  $s_0^{ab} = m_a m_b$ .

<sup>2</sup> In the left-hand side of the equation,  $a^+ \equiv a$  represents a positive-charge particle, while  $a^- \equiv \bar{a}$  corresponds to its negative-charge antiparticle.

<sup>3</sup> Actually, a constant term  $A_{\mathbb{P}}^{ab}$  could also originate from the sum of the *critical* (i.e., *simple-pole*) Pomeron with the constant term generated by higher-order singularities, e.g., a *triple-pole* Pomeron (which also gives a  $\ln^2 s$  term). In any case, however, its value is obviously affected by the choice of the energy scale in the leading and subleading terms in eq. (20) (see also the discussion at the end of this section).

Summarizing,  $A_i^{ab}$  (mb),  $b_i$  (dimensionless) and  $A_{\mathbb{P}}^{ab}$  (mb) are always free parameters to be determined in the fits. The parameters  $B$  (mb),  $C$  (mb) and  $\kappa$  (dimensionless) can be fixed or free, as detailed below in the descriptions of our variants of fits.

The names of the variants are written using the following notation: LT stands for **L**eading **T**erm, SLT for **S**ub **L**eading **T**erm, the subscript “th” refers to the case where we fix  $B$  (LT<sub>th</sub>) or both  $B$  and  $C$  (SLT<sub>th</sub>) to the theoretical values discussed in section II, and the subscript “ $\kappa$ ” indicates that the parameter  $\kappa$  is free. The variants considered here are the following:

- LT:  $C = 0$  and  $\kappa = 1$  are fixed parameters, while  $B$  is free. This case (in which the subleading term is absent) corresponds essentially to the parametrization used by the PDG in their analysis of forward data [34] and to the highest-rank result obtained by the COMPETE Collaboration [40] (see below for more details).
- SLT:  $\kappa = 1$  is fixed, while  $B$  and  $C$  are free parameters. This case corresponds to the previous parametrization with the inclusion of the subleading term.
- LT<sub>th</sub>:  $B = B_{\text{th}}$ ,  $C = 0$  and  $\kappa = 1$  are fixed parameters. This variant has  $B$  fixed to the theoretical values discussed in sec. II and no subleading term.
- SLT<sub>th</sub>:  $B = B_{\text{th}}$ ,  $C = C_{\text{th}}$  and  $\kappa = 1$  are fixed parameters. This variant has both  $B$  and  $C$  fixed to the theoretical values discussed in sec. II.
- SLT<sub>th, $\kappa$</sub> :  $B = B_{\text{th}}$  and  $C = C_{\text{th}}$  are fixed parameters, while  $\kappa$  is a free parameter.

The main difference between our LT parametrization, the highest-rank result by COMPETE, and the PDG parametrization, is in the energy scale appearing in the leading term  $\ln^2 s$ . In the COMPETE analysis, the energy scale  $s_0$  is a free parameter, which does not depend on the scattering particles. Our energy scale, on the other hand, is fixed and depends only on the masses of the scattering particles,  $s_0^{ab} = m_a m_b$ . In the PDG analysis this scale depends on the masses of the colliding particles and on a universal mass scale also entering their parametrization of the coefficient  $B$ , so it contains both a fixed and a free part. All in all, this results in the three parametrizations differing pairwise by a particle-dependent term of order  $\mathcal{O}(\ln s)$  (besides a particle-dependent constant term that can be reabsorbed in  $A_{\mathbb{P}}^{ab}$ ). Since very high-energy data are not yet available, this can affect the result obtained for  $B$  in the fits.

## IV. DATASET AND METHODOLOGY

In this section we describe our dataset and the methodology used in our fits.

### A. Dataset

Our dataset comprises data from meson-baryon and baryon-baryon scattering, namely  $pp$ ,  $\bar{p}p$ ,  $pn$ ,  $\bar{p}n$ ,  $\pi^\pm p$ ,  $K^\pm p$ ,  $K^\pm n$ , with cutoff energy  $\sqrt{s_{\min}} = 5$  GeV (so that we are well above the resonance region). This cutoff energy is the same used in the highest-rank result by the COMPETE Collaboration [40] and in the PDG analysis [34]. Only data obtained in accelerator experiments were included in the fits, i.e., no cosmic rays data were considered, and the datasets are those available at the PDG website [41].

For  $pp$  scattering, besides the data already in the PDG dataset at 7 TeV, we have included further data at 7 and 8 TeV obtained by the TOTEM and ATLAS Collaborations, namely, the luminosity-independent measurement at 7 TeV [10], the first measurement at 8 TeV [11] and the values of  $\sigma_{\text{tot}}$  obtained together with the  $\rho$  value at 8 TeV from the Coulomb-Nuclear interference region in the differential cross section data [12] by the TOTEM Collaboration, and the measurement at 7 TeV by the ATLAS Collaboration [13]. This information is summarized in table I. Our dataset therefore comprises data with energy in the range  $5 \text{ GeV} \leq \sqrt{s} \leq 8 \text{ TeV}$ .

Cosmic-ray data [42–44] are shown in the figures just to illustrate the trend with energy and, as stated above, they have not been included in the fits. Since their uncertainties are large, we expect that their inclusion in the fits would not change much the results. The energy range and the number of points available for each scattering channel that we have considered are shown in table II.

In all the cases, we have treated the datapoints as independent, including those that have the same energy. For all data we have considered statistic and systematic uncertainties added in quadrature.

We stress that we are not including data from reactions that involve photons or deuterons and we do not constrain our fits using the data for the  $\rho$  parameter, as it is done by COMPETE and PDG.

Finally, we mention that there are 9 points available for  $\Sigma^-p$  scattering in the energy

Table I: Experimental data of  $\sigma_{\text{tot}}$  in the LHC energy region.

$\sqrt{s}$ (TeV)	$\sigma_{\text{tot}}$ (mb)	Collaboration
7	$98.3 \pm 2.8$	TOTEM [8]
7	$98.6 \pm 2.2$	TOTEM [9]
7	$98.0 \pm 2.5$	TOTEM [10]
7	$99.1 \pm 4.1$	TOTEM [10]
7	$95.4 \pm 1.4$	ATLAS [13]
8	$101.7 \pm 2.9$	TOTEM [11]
8	$102.9 \pm 2.3$	TOTEM [12]
8	$103.0 \pm 2.3$	TOTEM [12]

Table II: Information about the reactions in our dataset: minimum energy, maximum energy and number of points for each reaction.

Reaction	$\sqrt{s_{\text{min}}}$ (GeV)	$\sqrt{s_{\text{max}}}$ (GeV)	# points
$pp$	5.01	8000	112
$\bar{p}p$	5.16	1800	59
$pn$	5.30	26.40	34
$\bar{p}n$	5.18	22.98	33
$\pi^+p$	5.21	25.28	50
$\pi^-p$	5.03	34.67	95
$K^+p$	5.13	24.14	40
$K^-p$	5.11	24.14	63
$K^+n$	5.24	24.16	28
$K^-n$	5.11	24.16	36
		Total:	559

region of interest [41]. Including these points makes the fits more unstable (due to the absence of data in the corresponding crossed channel), but this does not affect the results, because of their large errors. We have therefore decided not to include them in our analysis.

## B. Methodology

We first consider fits using our parametrization, eqs. (17) and (19)–(20), to data from  $pp$  and  $\bar{p}p$  scattering only. This pair of reactions constitutes the set with available data in the largest energy range. Since the subleading term of interest here is expected to be relevant at high energies, it is important to estimate its contribution without much weight from the low-energy data from other reactions. Nevertheless, we have also considered fits to all the data for the hadron-hadron processes shown in table II.

In order to start from a solid and updated result, we decided to use as initial values for the LT fit the results presented in PDG 2016 [34], and then use the results of LT as initial values for the SLT fit. In this way, fitting first LT (that essentially corresponds to the PDG parametrization, as we have already observed above) we create a reference for discussing differences when we include the subleading term as well (SLT), instead of comparing directly to the PDG result. This procedure, however, turned out to be problematic in the fit to all hadronic data (see below sec. VB1). In that case we therefore decided to use as initial values for the parameters  $B$  and  $C$  in the SLT fit to all data the results obtained in the SLT fit to  $pp/\bar{p}p$  data. For the other parameters, we used the results obtained in the LT fit to all data. The detailed scheme is shown in fig. 1, where  $X \rightarrow Y$  means that the results of variant  $X$  were used as initial values for the fit with variant  $Y$ .

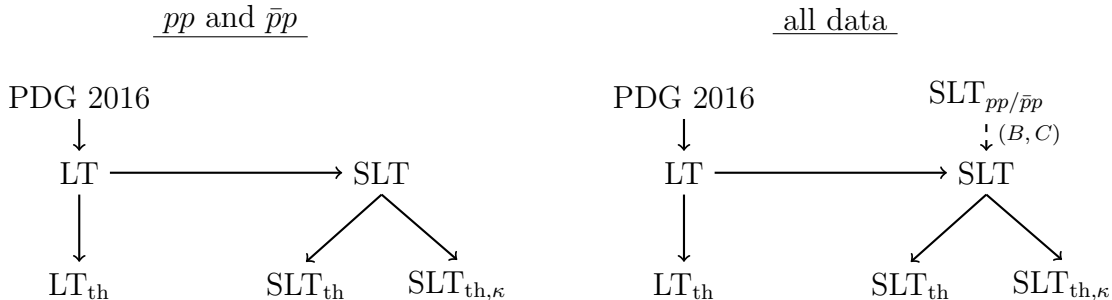


Figure 1: Initial-value scheme used in the fits.

We use the reduced chi-squared ( $\chi^2/\nu$ , where  $\nu$  is the number of degrees of freedom) as a measure of the quality of the fit [45, 46]. However, we do not base our preference for a result over another on small differences in the value of this quantity, since the inclusion of both statistical and systematic uncertainties puts some limits on the use of this test. It is important to note that some data obtained by the TOTEM Collaboration do not have

statistical uncertainty (as can be seen in the caption of table 1 in Ref. [10]).

The fits were performed with the class TMinuit from the ROOT Framework [47] with  $1\sigma$  of confidence level.

## V. FIT RESULTS

In this section we present the results obtained in our fits, first to  $pp$  and  $\bar{p}p$  data only, and later to all reactions, considering all variants described above in sec. III. Finally, we compare and discuss our results.

### A. Fits to $pp$ and $\bar{p}p$ Data

The parameters obtained in fits to  $pp$  and  $\bar{p}p$  data with LT and SLT are shown in table III, those with  $LT_{\text{th}}$ ,  $SLT_{\text{th}}$  and  $SLT_{\text{th},\kappa}$  in table IV. The curves calculated with these parameters are compared with the experimental data in figs. 2, 3 and 4. Below we discuss the results that we have obtained using the different variants.

#### 1. Fits with LT and SLT

The results obtained with variants LT and SLT provide a good description of the experimental data. Although there is a small decrease in the value of  $\chi^2/\nu$  going from LT to SLT, nevertheless, as discussed in section IV B, we cannot favor one variant over the other on the basis of this value. Given that both are  $\lesssim 1$ , we can say that both variants result in good fits to the data.

Interestingly enough, the LT fit yields for  $B$  a value close to the theoretical prediction  $B_{\text{th}}$  obtained in Ref. [14] using the mass and spin of the  $\Omega^\pm$  baryon.

With SLT we have obtained  $C < 0$  and  $C \neq 0$  within the uncertainty. The negative value of  $C$  causes an increase in the  $B$  parameter and also in  $A_{\mathbb{P}}$  to compensate for the negative contribution of the subleading term. The uncertainty on  $A_{\mathbb{P}}$  increases one order of magnitude, but the relative uncertainty is still small ( $\sim 5.6\%$ ).

Given the small difference mentioned above between the values of  $\chi^2/\nu$  obtained with LT and SLT, we cannot claim that the fit with the subleading term represents an improvement

Table III: Results of fits with LT and SLT to  $\sigma_{\text{tot}}$  data of  $pp$  and  $\bar{p}p$  scattering. Parameters  $A_1, A_2, A_{\mathbb{P}}, B, C$  are in mb, while  $b_1, b_2$  and  $\kappa$  are dimensionless.

	Fits to $\sigma_{\text{tot}}$	
	LT	SLT
$B$	0.2269(38)	0.349(29)
$C$	0 (fixed)	-0.95(21)
$b_1$	0.342(15)	0.560(76)
$b_2$	0.539(15)	0.541(16)
$\kappa$	1 (fixed)	1 (fixed)
$A_1$	56.8(1.7)	64.4(8.2)
$A_2$	35.2(2.5)	35.6(2.5)
$A_{\mathbb{P}}$	24.77(60)	35.7(2.0)
$\chi^2/\nu$	0.972	0.933
$\nu$	165	164

over the fit without it. We can only say that the data are compatible with a nonzero value of  $C$ .

Regarding the Reggeon trajectories, the values of  $b_1$  and  $b_2$  obtained in LT are not far from the values obtained by the PDG and also in other analyses (such as, for example, the one by Menon and Silva in Ref. [48]). When changing from LT to SLT, i.e., allowing  $C$  to be nonzero, we find that  $A_2$  and  $b_2$  are practically stable, while  $A_1$  and  $b_1$  increase; moreover, we observe that the values of  $b_1$  and  $b_2$  are compatible within the errors, i.e., the intercepts of the two Reggeon trajectories become degenerate. A similar effect was observed by COMPETE in Ref. [40], when discussing their highest-rank result (similar to LT). In that case, the degeneracy of the Reggeon intercepts was ascribed to a decreasing contribution of the log-squared term for  $s < s_h$ , where  $s_h$  is the energy scale determined in the fit.

In Ref. [23], Díez, Godbole and Sinha performed fits to  $\sigma_{\text{tot}}$  data from  $pp$  and  $\bar{p}p$  scattering in order to determine what is the dominant subleading contribution to  $\sigma_{\text{tot}}$  between  $\ln s$  and  $\ln s \ln \ln s$  (see section II). They also parametrize the low-energy contributions to  $\sigma_{\text{tot}}$  with Reggeon terms, however fixing some of the parameters according to the expectations from

Regge theory, and some others using sum rules in the resonance region (following the works by Block and Halzen [49]). Their analysis favors the  $\ln s$  term over the  $\ln s \ln \ln s$  one. Their approach differs from ours mainly in two aspects: (i) they fix low-energy parameters, which we do not, and (ii) they do not address the question of the dependence on the colliding particles, while in Ref. [14] it is argued that the  $\ln s \ln \ln s$  is universal, while the  $\ln s$  term is reaction dependent.

In the present analysis we want to investigate only the universal terms, leaving the  $\ln s$  contribution to a future study. In fact, the inclusion of this kind of term would increase the number of free parameters, especially in the fits to all reactions. We think that for the time being it is better to keep the fits as simple as possible and avoid a large number of parameters.

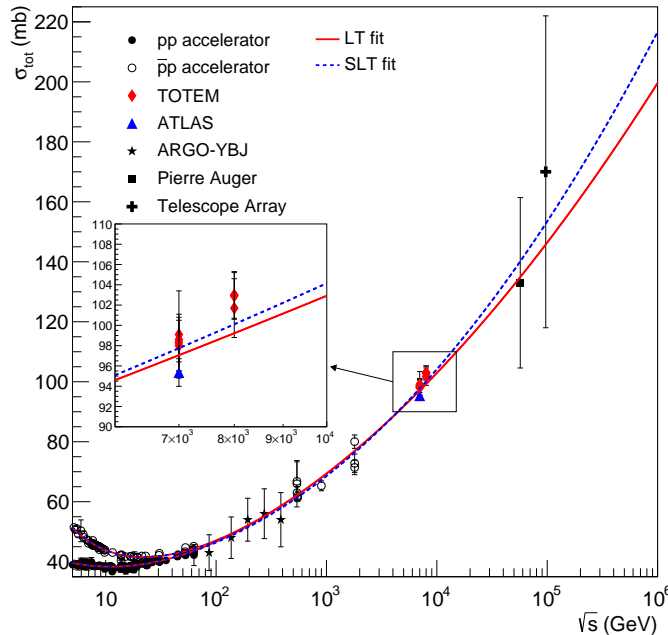


Figure 2: Results of fits with LT and SLT to  $pp$  and  $\bar{p}p$  data.

2. *Fits with  $LT_{th}$  ( $\kappa = 1, B = B_{th}, C = 0$ ),  $SLT_{th}$  ( $\kappa = 1, B = B_{th}, C = C_{th}$ ) and  $SLT_{th,\kappa}$  ( $\kappa$  free,  $B = B_{th}, C = C_{th}$ )*

After performing the fits with LT and SLT, we did fits where  $B$  and  $C$  were fixed to the values discussed in section II. In table IV we divide the results according to the variants and to the values of  $B$  and  $C$  used.

*a. Fits with  $LT_{th}$  and  $SLT_{th}$ :  $B$  and  $C$  from the  $\Omega^\pm$  baryon.* The values of  $B$  and  $C$  calculated with the mass and spin of the  $\Omega^\pm$  baryon [eq. (12)] are  $B_{th} = 0.22$  mb and  $C_{th} = -0.44$  mb. In  $LT_{th}$  we have  $B = B_{th}$  and  $C = 0$  fixed. The result obtained (2nd column of table IV) is close to the one obtained using  $LT$ . This is not surprising, given that in that case, (see table III) one finds  $B = 0.2269$  mb  $\sim 0.23$  mb, close to  $B_{th}$ , as we have already remarked. The other parameters and the value of  $\chi^2/\nu$  present small variations compared to  $LT$ . We also have a good description of the experimental data (see figure 3).

On the other hand, in  $SLT_{th}$ , where now  $C = C_{th}$  is fixed, the result is not satisfactory as with the previous variant. In fact, the value of  $\chi^2/\nu$  is considerably high, indicating a poor description of the data. This can be seen in figure 3: the curve obtained from the fit does not describe data with  $\sqrt{s} \gtrsim 1$  TeV. We would like to point out that we have practically no change in the parameters associated with the odd signature Reggeon contribution, while the intercept of the even trajectory increases going from  $LT_{th}$  to  $SLT_{th}$ . The same happens to  $A_1$ .

*b. Fits with  $LT_{th}$  and  $SLT_{th}$ :  $B$  and  $C$  from the  $2^{++}$  glueball state.* In this case, we consider the (quenched) mass and spin of the  $2^{++}$  glueball state, giving  $B_{th} = -C_{th} = 0.42$  mb [eq. (13)]. With both variants we get a poor description of the data with  $\chi^2/\nu \sim 3$ . Besides this, the fits present a non-positive-definite error matrix. In this case, although the fit has converged, we cannot fully trust the uncertainties estimated for the free parameters [45], and so the results of our fit in general. For these reasons we have decided not to show the results in table IV. For the sake of completeness, we mention that the intercept  $b_1$  of the even Reggeon trajectory is very small compared with that obtained in the other cases and that we have a negative ‘‘constant’’ Pomeron contribution ( $A_P < 0$ ).

The description of data are similar for the two variants, with overestimation of  $\sigma_{tot}$  at LHC energies.

*c. Fits with  $LT_{th}$  and  $SLT_{th}$ :  $B$  and  $C$  from the  $3^{+-}$  glueball state.* Considering the  $3^{+-}$  glueball state, we have (using again the quenched mass)  $B_{th} = 0.78$  mb and  $C_{th} = -0.39$  mb [see eq. (14)]. In these cases, the minimizer did not converge and, therefore, no fit results were obtained.

*d. Fits with  $SLT_{th,\kappa}$  ( $\kappa$  free,  $B = B_{th}$ ,  $C = C_{th}$ ).* In these variants we consider both  $B$  and  $C$  fixed with  $\kappa$  free. The parameters obtained with these fits are shown in table IV. With these variants we can estimate which of the scenarios discussed after eq. (16) is realized

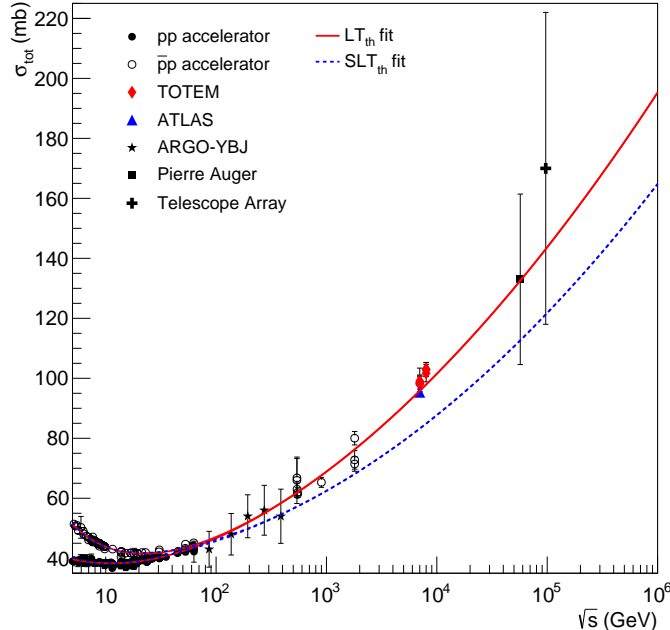


Figure 3: Results of fits with  $LT_{th}$  ( $\kappa = 1$ ,  $B = B_{th}$ ,  $C = 0$ ) and  $SLT_{th}$  ( $\kappa = 1$ ,  $B = B_{th}$ ,  $C = C_{th}$ ) to  $pp$  and  $\bar{p}p$  data for  $B_{th}$  and  $C_{th}$  calculated from the  $\Omega^\pm$  baryon.

at asymptotically high energies, since according to eq. (16) the asymptotic ratio between  $\sigma_{el}$  and  $\sigma_{tot}$  is given by  $\kappa/2$ .

In all the cases considered for the  $B_{th}$  and  $C_{th}$  values, the fits are of good quality ( $\chi^2/\nu \lesssim 1$ ) with small differences in the  $\chi^2$  value among them. We see small variations of some parameters, for instance,  $A_1$ ,  $b_1$  and  $A_p$ . Apart from these differences, the quality of the matching between the fitted curve and the experimental data is the same in the fitted energy range for all cases. Indeed, as can be seen in the inset of fig. 4, the difference at LHC energies is very small and the results start to be appreciably different only at cosmic-ray energies.

Regarding the value of  $\kappa$ , using the values of  $B_{th}$  and  $C_{th}$  obtained from the  $\Omega^\pm$  baryon, we get  $\kappa > 1$ , therefore an *antishadowing* scenario. For the glueball cases, we get  $\kappa < 1$ , hence a *grey-disk* scenario, the value obtained with the  $2^{++}$  glueball being larger than that obtained with the  $3^{+-}$ .

## B. Fits to All Reactions

In this section we present and discuss the results obtained from fits to the full dataset (data from meson-baryon and baryon-baryon scattering) with the variants LT and SLT

Table IV: Results of fits with  $LT_{\text{th}}$  ( $\kappa = 1$ ,  $B = B_{\text{th}}$ ,  $C = 0$ ),  $SLT_{\text{th}}$  ( $\kappa = 1$ ,  $B = B_{\text{th}}$ ,  $C = C_{\text{th}}$ ) and  $SLT_{\text{th},\kappa}$  ( $\kappa$  free,  $B = B_{\text{th}}$ ,  $C = C_{\text{th}}$ ) to  $\sigma_{\text{tot}}$  data of  $pp$  and  $\bar{p}p$  scattering. The values of  $B$  and  $C$  are fixed to the theoretical values calculated with the masses and the spins of the  $\Omega^\pm$  baryon, the  $2^{++}$  glueball state and the  $3^{+-}$  glueball state (quenched values). For the units of measurement of the parameters, see table III.

	$\Omega^\pm$ baryon			$2^{++}$ glueball	$3^{+-}$ glueball
	$LT_{\text{th}}$	$SLT_{\text{th}}$	$SLT_{\text{th},\kappa}$	$SLT_{\text{th},\kappa}$	$SLT_{\text{th},\kappa}$
$B$	0.22 (fixed)	0.22 (fixed)	0.22 (fixed)	0.42 (fixed)	0.78 (fixed)
$C$	0 (fixed)	-0.44 (fixed)	-0.44 (fixed)	-0.42 (fixed)	-0.39 (fixed)
$b_1$	0.365(10)	0.743(20)	0.548(20)	0.385(17)	0.361(17)
$b_2$	0.539(15)	0.528(16)	0.540(15)	0.539(15)	0.539(15)
$\kappa$	1 (fixed)	1 (fixed)	1.377(18)	0.6159(96)	0.3097(51)
$A_1$	58.5(1.7)	115.3(8.5)	57.5(3.2)	56.0(2.2)	56.3(2.0)
$A_2$	35.3(2.5)	33.7(2.4)	35.4(2.5)	35.3(2.4)	35.2(2.4)
$A_{\mathbb{P}}$	25.75(21)	35.862(74)	32.17(29)	28.13(46)	26.38(55)
$\chi^2/\nu$	0.987	3.59	0.937	0.957	0.965
$\nu$	166	166	165	165	165

(table V) and with the variants  $LT_{\text{th}}$ ,  $SLT_{\text{th}}$  and  $SLT_{\text{th},\kappa}$  (table VI). The comparison of the corresponding curves with the experimental data is shown in figs. 5, 6 and 7.

### 1. Fits with $LT$ and $SLT$

The results are presented in table V and in figure 5. With the  $LT$  variant we obtain a good description of the data with  $\chi^2/\nu \sim 1$ . The same is true for  $SLT$ , that we now discuss in some detail.

As already mentioned above in section IV B, the  $SLT$  fit requires some care. Following the same scheme for the choice of initial values as in the analysis of  $pp$  and  $\bar{p}p$  data (see fig. 1), the resulting fit has a non-positive-definite error matrix. We therefore decided to use the values obtained for the parameters  $B$  and  $C$  in the fit to  $pp$  and  $\bar{p}p$  data with the  $SLT$  (table III) instead of the values obtained in the  $LT$  fit to all reactions. Namely, we used as

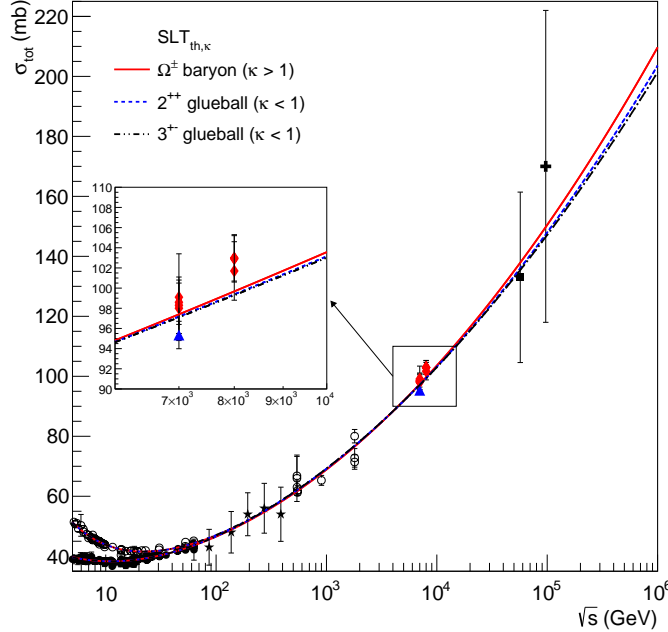


Figure 4: Results of fits with  $SLT_{th,\kappa}$  ( $\kappa$  free,  $B = B_{th}$ ,  $C = C_{th}$ ) to  $pp$  and  $\bar{p}p$  data for  $B_{th}$  and  $C_{th}$  calculated from the  $\Omega^\pm$  baryon, and the  $2^{++}$  and  $3^{+-}$  glueball states. The legend of data is the same of figure 2.

initial values  $B = 0.349$  mb and  $C = -0.95$  mb instead of  $B = 0.2433$  mb and  $C = 0$ . For the other parameters the initial values remain unchanged, i.e., we used the values obtained in the LT fit to all data. With this choice we obtained a more reliable result with an accurate error matrix. In the SLT fit to all data we find again  $C < 0$ , but with smaller magnitude and uncertainty than in the SLT fit to  $pp$  and  $\bar{p}p$  data, although the relative uncertainty is the same ( $\sim 22\%$ ). We attribute this to the presence of more data at low energies. On the other hand, the  $\chi^2/\nu$  is practically the same. It is important to mention that here we are increasing the effect of low-energy data in the estimation of  $C$  compared to the  $pp/\bar{p}p$  fits, since we have more low-energy than high-energy data points in the present dataset. In fact, we have non-zero correlation coefficients between low- and high-energy parameters, indicating the influence of the low-energy data in the determination of  $C$  in the fit (see also table 6 in Ref. [50]).

Apart from these general aspects of the fits, there is still one point that demands some comments. This point concerns the negative value of the parameter  $A_p^{\pi p}$  that appears in LT, while it changes to a positive value in SLT. This is the only negative constant Pomeron contribution (although with large errors) in this set of fits. Taking into account the property

of factorization of the residues of the Regge poles [7] (see also the comments in Ref. [40]), this parameter is expected to be positive. However, factorization is only proven in the case of simple poles and it is valid when only one trajectory dominates [7]. As already commented in footnote 3 in sec. III,  $A_{\mathbb{P}}^{ab}$  could also originate from the sum of a constant (simple-pole) Pomeron with the constant term coming from higher-order singularities (e.g., a triple-pole Pomeron) and, in any case (see also the discussion at the end of sec. III), its value is affected by the choice of the energy scale in the leading and subleading terms in eq. (20). Therefore, we cannot exclude this result only on the basis of factorization. On the other hand, even with  $A_{\mathbb{P}}^{\pi p} < 0$ , we do not have a negative Pomeron contribution (from the combination of this constant term plus the  $\ln^2 s$  term) in LT.

2. *Fits with  $LT_{th}$  ( $\kappa = 1, B = B_{th}, C = 0$ ),  $SLT_{th}$  ( $\kappa = 1, B = B_{th}, C = C_{th}$ ) and  $SLT_{th,\kappa}$  ( $\kappa$  free,  $B = B_{th}, C = C_{th}$ )*

In table VI we present the results obtained with the variants  $LT_{th}$  and  $SLT_{th}$ , where  $B$  and  $C$  are fixed to their theoretical values [see eqs. (12)–(14)].

a. *Fits with  $LT_{th}$  and  $SLT_{th}$ :  $B$  and  $C$  from the  $\Omega^\pm$  baryon.* The results (2nd and 3rd column of table VI) obtained in this case are satisfactory for  $LT_{th}$  with only a small increase of  $\chi^2/\nu$  in comparison with LT. For  $SLT_{th}$ , we get  $\chi^2/\nu \sim 2$  while in SLT we have  $\sim 1$ . However, this increase is less than that observed in the fits to  $pp$  and  $\bar{p}p$  data only. Contrary to the LT fit, we have that all  $A_{\mathbb{P}}^i > 0$  in  $LT_{th}$ .

Regarding the comparison with the data,  $LT_{th}$  gives a good description of them, favoring the ATLAS point at 7 TeV in  $pp/\bar{p}p$ , while  $SLT_{th}$  does not seem to describe well the  $pp/\bar{p}p$  data with  $\sqrt{s} \gtrsim 500$  GeV (see fig. 6). Concerning the other reactions (where data are at much lower energies than in the  $pp/\bar{p}p$  case), both  $LT_{th}$  and  $SLT_{th}$  seem to describe data reasonably well (even if, of course, the two variants have a quite different high-energy behavior).

b. *Fits with  $LT_{th}$  and  $SLT_{th}$ :  $B$  and  $C$  from the  $2^{++}$  glueball state.* The fits with  $LT_{th}$  and  $SLT_{th}$  in this case have a non-positive-definite error matrix. The results (not presented in table VI) have the same features of the fits to  $pp$  and  $\bar{p}p$  data, for example, a very small  $b_1$  parameter. We also have that almost all  $A_{\mathbb{P}}^i < 0$ . The  $\chi^2/\nu$  values are around 1.5, with a similar quality in the matching with data for both variants. Regarding  $pp$  and  $\bar{p}p$ , the fits

Table V: Results of fits with LT and SLT to  $\sigma_{\text{tot}}$  (all data). For the units of measurement of the parameters, see table III.

	LT	SLT
$B$	0.2433(46)	0.2652(96)
$C$	0 (fixed)	-0.200(44)
$b_1$	0.222(11)	0.2420(85)
$b_2$	0.5128(99)	0.513(11)
$\kappa$	1 (fixed)	1 (fixed)
$A_1^{pp}$	47.86(62)	44.33(91)
$A_2^{pp}$	30.8(1.4)	30.8(1.5)
$A_{\mathbb{P}}^{pp}$	19.0(1.1)	22.61(22)
$A_1^{pn}$	47.2(1.1)	43.6(1.3)
$A_2^{pn}$	27.4(1.5)	27.5(1.6)
$A_{\mathbb{P}}^{pn}$	19.2(1.1)	22.86(36)
$A_1^{\pi p}$	70.37(99)	67.9(1.7)
$A_2^{\pi p}$	15.7(1.0)	15.8(1.1)
$A_{\mathbb{P}}^{\pi p}$	-3.3(1.3)	0.80(31)
$A_1^{Kp}$	3.42(57)	30.31(73)
$A_2^{Kp}$	17.54(91)	17.56(96)
$A_{\mathbb{P}}^{Kp}$	1.77(85)	5.09(11)
$A_1^{Kn}$	32.72(73)	28.76(77)
$A_2^{Kn}$	9.28(69)	9.30(71)
$A_{\mathbb{P}}^{Kn}$	1.93(84)	5.22(14)
$\chi^2/\nu$	1.060	1.063
$\nu$	532	531

overestimate the data at LHC energies, reaching the upper error bar of the TOTEM data.

*c. Fits with  $LT_{th}$  and  $SLT_{th}$ :  $B$  and  $C$  from the  $3^{+-}$  glueball state.* Again, using the mass and spin of the  $3^{+-}$  glueball state, the fits did not converge.

Table VI: Results of fits with  $LT_{\text{th}}$  ( $\kappa = 1$ ,  $B = B_{\text{th}}$ ,  $C = 0$ ),  $SLT_{\text{th}}$  ( $\kappa = 1$ ,  $B = B_{\text{th}}$ ,  $C = C_{\text{th}}$ ) and  $SLT_{\text{th},\kappa}$  ( $\kappa$  free,  $B = B_{\text{th}}$ ,  $C = C_{\text{th}}$ ) to  $\sigma_{\text{tot}}$  (all data). The values of  $B$  and  $C$  are fixed to the theoretical values calculated with the masses and the spins of the  $\Omega^\pm$  baryon, the  $2^{++}$  glueball state and the  $3^{+-}$  glueball state (quenched values). For the units of measurement of the parameters, see table III.

	$\Omega^\pm$ baryon			$2^{++}$ glueball	$3^{+-}$ glueball
	$LT_{\text{th}}$	$SLT_{\text{th}}$	$SLT_{\text{th},\kappa}$	$SLT_{\text{th},\kappa}$	$SLT_{\text{th},\kappa}$
$B$	0.22 (fixed)	0.22 (fixed)	0.22 (fixed)	0.42 (fixed)	0.78 (fixed)
$C$	0 (fixed)	-0.44 (fixed)	-0.44 (fixed)	-0.42 (fixed)	-0.39 (fixed)
$b_1$	0.2744(66)	0.554(13)	0.292(14)	0.249(13)	0.234(12)
$b_2$	0.5141(97)	0.515(11)	0.514(10)	0.513(11)	0.513(11)
$\kappa$	1 (fixed)	1 (fixed)	1.439(23)	0.653(12)	0.3303(64)
$A_1^{pp}$	47.04(71)	59.0(2.7)	37.99(87)	43.12(57)	45.54(58)
$A_2^{pp}$	31.0(1.4)	31.4(1.6)	30.9(1.4)	30.8(1.5)	30.8(1.5)
$A_{\mathbb{P}}^{pp}$	23.40(24)	35.159(77)	29.22(51)	23.76(82)	21.29(98)
$A_1^{pn}$	46.3(1.2)	57.8(3.2)	37.3(1.2)	42.4(1.1)	44.9(1.1)
$A_2^{pn}$	27.6(1.5)	27.9(1.7)	27.5(1.6)	27.5(1.6)	27.4(1.6)
$A_{\mathbb{P}}^{pn}$	23.64(37)	35.24(15)	29.44(56)	24.01(87)	21.5(1.0)
$A_1^{\pi p}$	73.5(1.5)	136.9(8.2)	64.8(2.3)	67.0(1.5)	68.6(1.2)
$A_2^{\pi p}$	16.11(98)	16.7(1.1)	16.1(1.0)	15.9(1.1)	15.8(1.1)
$A_{\mathbb{P}}^{\pi p}$	19.84(28)	15.921(83)	8.27(65)	20.8(1.0)	-0.69(1.2)
$A_1^{Kp}$	32.53(51)	28.1(1.4)	22.61(49)	28.95(47)	31.68(54)
$A_2^{Kp}$	17.67(88)	17.66(98)	17.57(92)	17.55(96)	17.54(97)
$A_{\mathbb{P}}^{Kp}$	5.39(18)	15.450(48)	11.09(37)	6.15(64)	3.90(78)
$A_1^{Kn}$	30.89(72)	23.8(1.8)	20.86(64)	27.38(71)	30.16(72)
$A_2^{Kn}$	9.35(69)	9.43(73)	9.33(70)	9.30(71)	9.29(72)
$A_{\mathbb{P}}^{Kn}$	5.48(20)	15.388(71)	11.18(36)	6.27(64)	4.04(77)
$\chi^2/\nu$	1.108	1.966	1.071	1.062	1.061
$\nu$	533	533	532	532	532

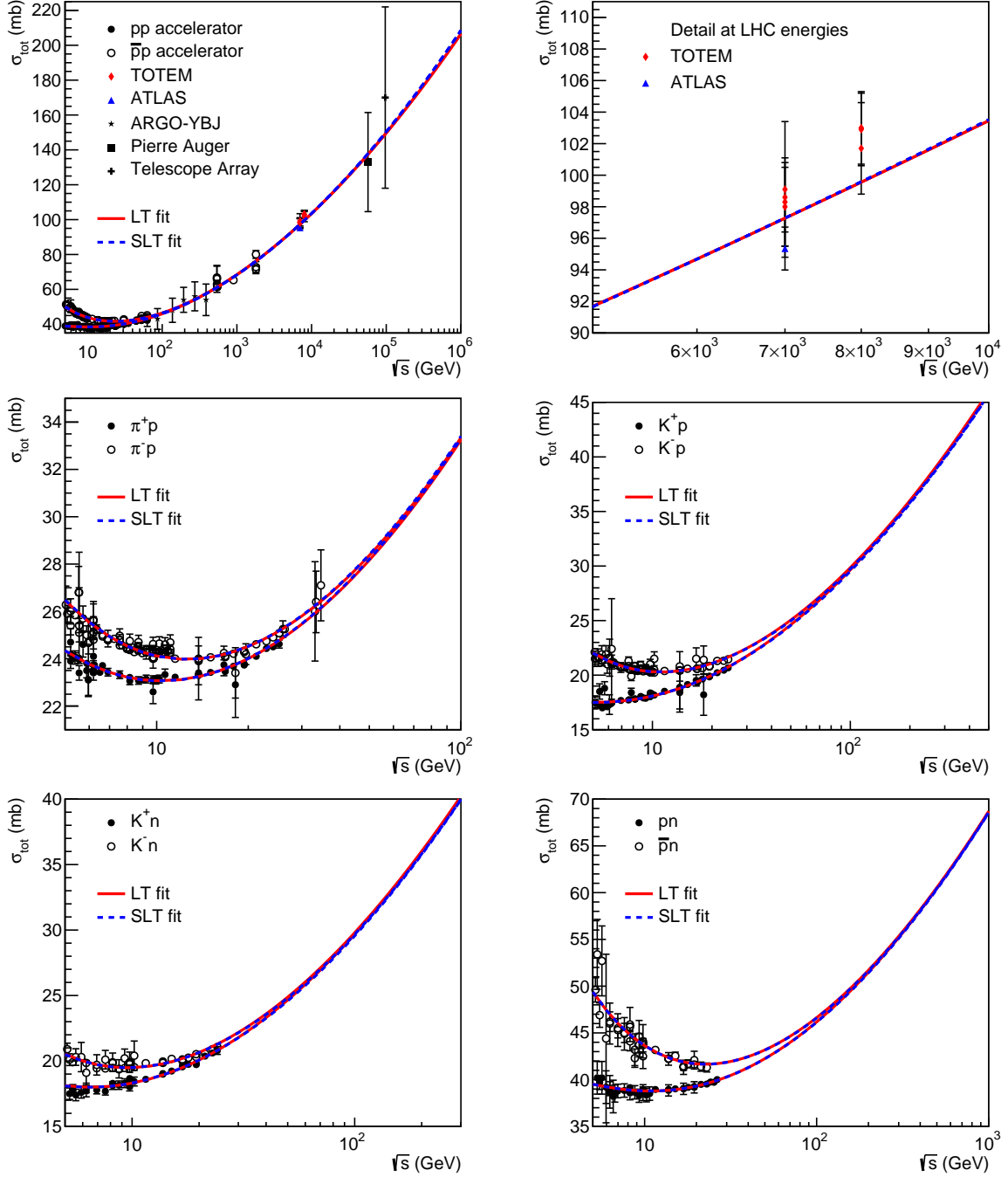


Figure 5: Results of fits with LT and SLT to all data.

*d. Fits with  $SLT_{th,\kappa}$  ( $\kappa$  free,  $B = B_{th}$ ,  $C = C_{th}$ ).* Finally we discuss the results of the fits where  $\kappa$  is a free parameter. We show in table VI all the parameters determined in the fits. The  $\chi^2/\nu$  values are close to 1, indicating that the fit is of good quality. Furthermore, we get a good description of data in all cases. As in the fit with SLT, the “constant” Pomeron term  $A_{\mathbb{P}}^{\pi p}$  is positive, except when we consider the  $3^{+-}$  glueball state, in which case we find

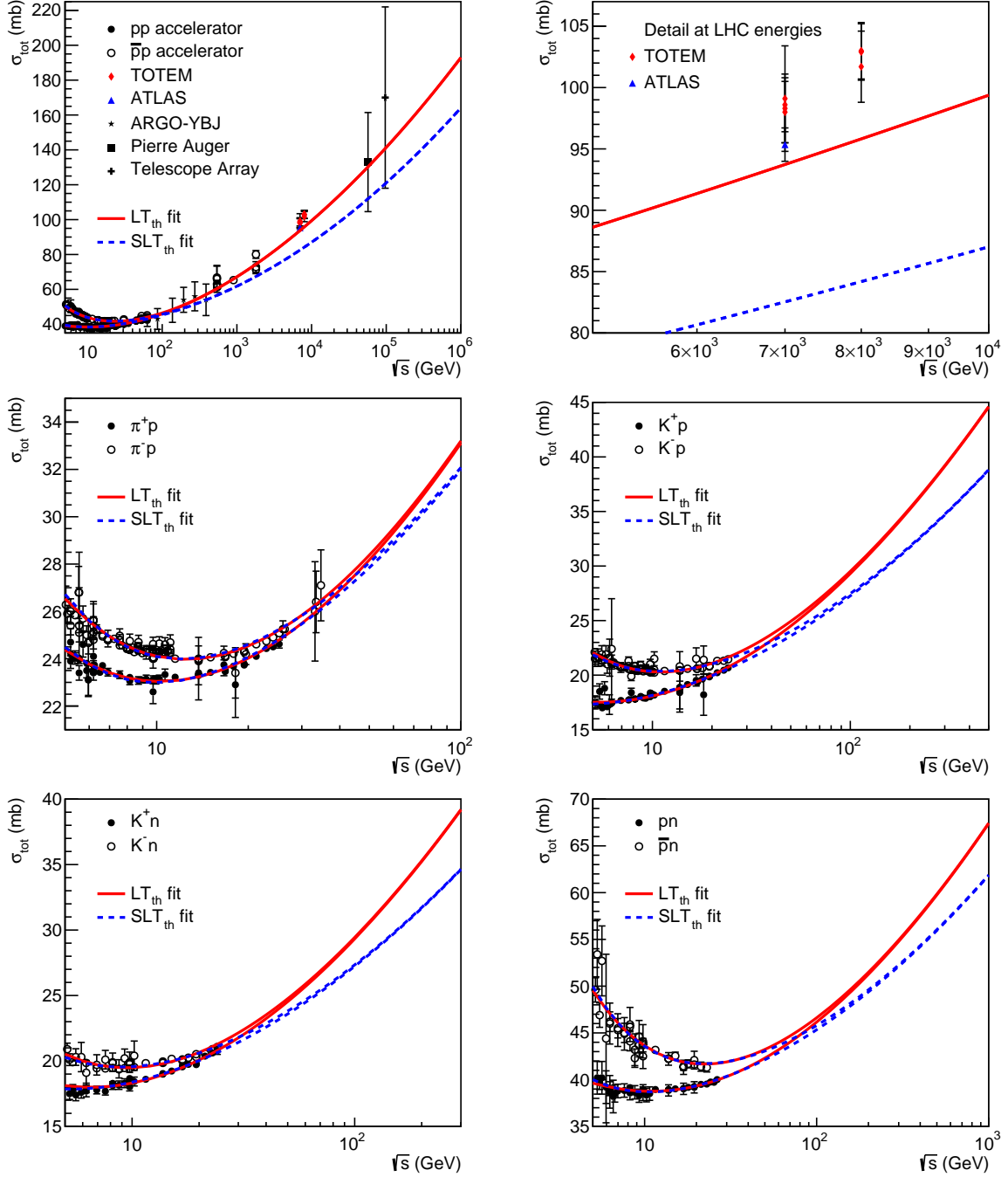


Figure 6: Results of fits with  $LT_{th}$  ( $\kappa = 1$ ,  $B = B_{th}$ ,  $C = 0$ ) and  $SLT_{th}$  ( $\kappa = 1$ ,  $B = B_{th}$ ,  $C = C_{th}$ ) to all data for  $B_{th}$  and  $C_{th}$  calculated from the  $\Omega^\pm$  baryon.

a negative central value, which is however compatible with zero.

The agreement between the fitted curve and the data (fig. 7) is also similar to that achieved when fitting only the  $pp$  and  $\bar{p}p$  data: in the energy range of the fit all cases give almost indistinguishable curves, which present small differences in the extrapolation to

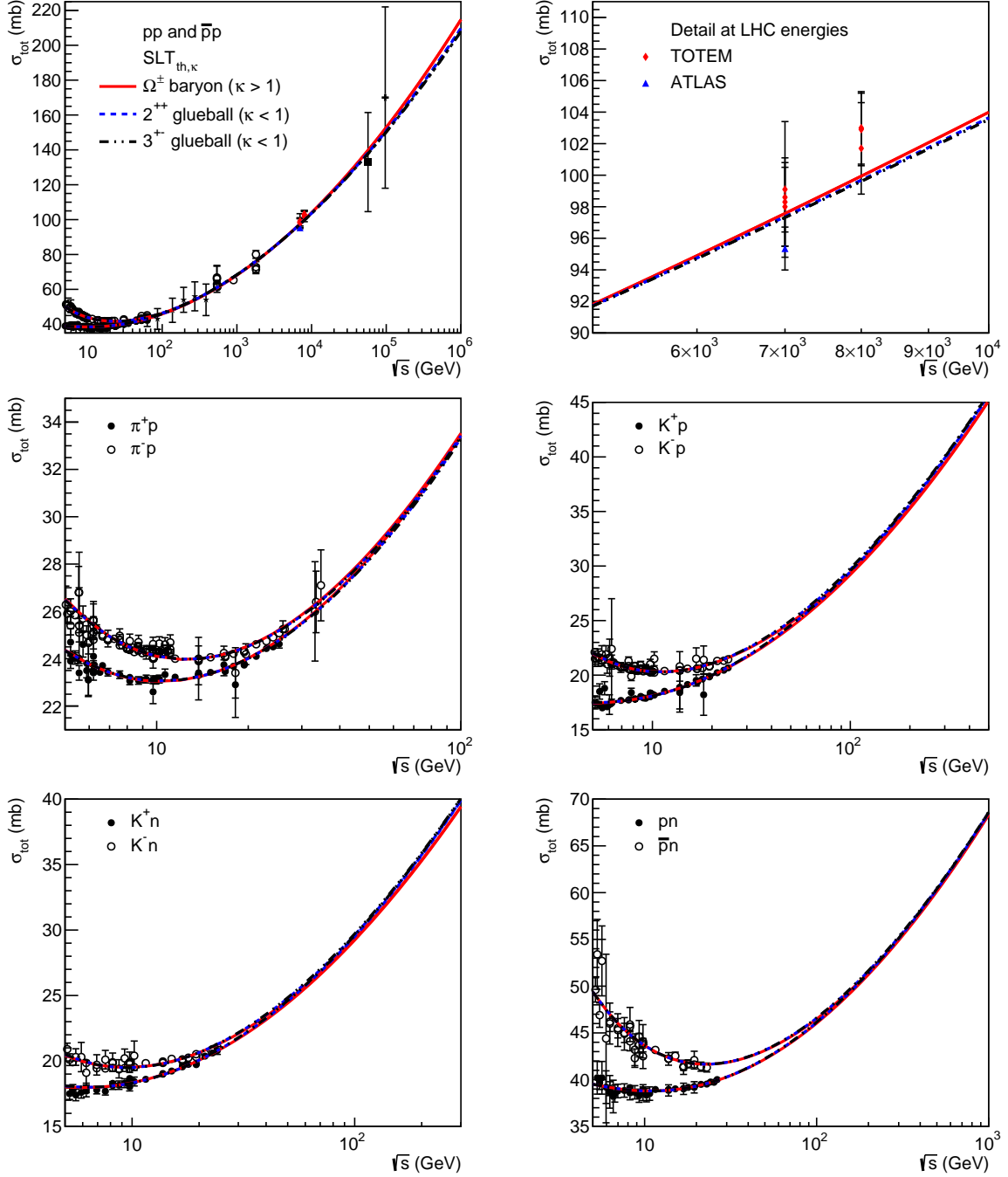


Figure 7: Results of fits with  $SLT_{th,\kappa}$  ( $\kappa$  free,  $B = B_{th}$ ,  $C = C_{th}$ ) to all data for  $B_{th}$  and  $C_{th}$  calculated from the  $\Omega^\pm$  baryon, and the  $2^{++}$  and  $3^{+-}$  glueball states. The legend for the curves is shown in the top-left panel. For the legend of  $pp$  and  $\bar{p}p$  data see figure 2.

higher energies. In conclusion, the three choices for  $B_{th}$  and  $C_{th}$  all give equally good fits.

Concerning the parameter  $\kappa$ , we have  $\kappa > 1$  for the  $\Omega^\pm$  baryon and  $\kappa < 1$  for the  $2^{++}$  and  $3^{+-}$  glueball states (with smaller  $\kappa$  in the latter case), as it was also found when fitting

$pp$  and  $\bar{p}p$  data only, but with slightly bigger central values.

## VI. CONCLUSIONS

In this work we have performed a phenomenological analysis of total cross section data from hadronic scattering in order to estimate the relevance of a subleading  $\ln(s/s_0) \ln \ln(s/s_0)$  term, obtained in recent theoretical studies in nonperturbative QCD [14] (see also Refs. [21–23] for a similar subleading term). More precisely, we used the following parametrization of the total cross section in the high-energy region:

$$\sigma_{\text{tot}}^{ab}(s) \underset{s \rightarrow \infty}{\sim} B \ln^2 \left( \frac{s}{s_0^{ab}} \right) + C \ln \left( \frac{s}{s_0^{ab}} \right) \ln \left[ \ln \left( \frac{s}{s_0^{ab}} \right) \right], \quad (21)$$

with  $s_0^{ab} = m_a m_b$ . The low-energy region was parametrized as usual in terms of Reggeon exchange in the  $t$ -channel.

We have determined the parameters  $B$  and  $C$  through fits (SLT fits) to two datasets with total center-of-mass energy  $\sqrt{s} \geq 5$  GeV: (i) only  $pp$  and  $\bar{p}p$  scattering and (ii) all meson-baryon and baryon-baryon data available at the PDG website [41] (except for  $\Sigma^- p$ ). In both cases, the recent data for  $pp$  scattering obtained at 7 and 8 TeV by the TOTEM and ATLAS Collaborations [8–13] were included in the fits. In the first case we have obtained  $B_{pp} = 0.349 \pm 0.029$  mb and  $C_{pp} = -0.95 \pm 0.21$  mb, while in the second case  $B_{\text{all}} = 0.2652 \pm 0.0096$  mb and  $C_{\text{all}} = -0.200 \pm 0.044$  mb. Both fits result in a good and equivalent description of the experimental data. However, we note that  $B_{pp}$ ,  $C_{pp}$  and  $B_{\text{all}}$ ,  $C_{\text{all}}$  are not compatible. We can understand this difference from the fact that when all reactions are considered we have more data in the low-energy region, since most of the data of meson-baryon and baryon-baryon scattering are available for  $\sqrt{s} \lesssim 25$  GeV, and this strongly affects the central value. In any case, it is important to keep in mind that the result reported in eq. (21) is asymptotic and that the contribution of this subleading term may still be weak, and so difficult to identify, in the LHC energy region.

As discussed in section II, the parameters  $B$  and  $C$  may be written, following the nonperturbative QCD approach of Ref. [14], in terms of the spin  $\tilde{s}$  and the mass  $\tilde{m}$  of the particle that maximizes the ratio of eq. (7). This yields (apart from a common multiplicative constant  $\kappa$ ) what we have called  $B_{\text{th}}$  and  $C_{\text{th}}$  [eq. (10)]. While in Ref. [14]  $B_{\text{th}}$  and  $C_{\text{th}}$  were estimated from the hadronic spectrum, here we can try to reverse the approach, and estimate

$\tilde{s}$  and  $\tilde{m}$  from the values of  $B$  and  $C$  obtained with the SLT fit. Equating the values of  $B$  and  $C$  in eq. (21) to  $\kappa B_{\text{th}}$  and  $\kappa C_{\text{th}}$ , respectively, we find that:

$$\tilde{s} = 1 - \frac{B}{C} \quad \text{and} \quad \frac{\tilde{m}^2}{\kappa} = 2\pi \frac{B}{C^2}. \quad (22)$$

Of course, we are not able to determine all the three parameters  $\kappa$ ,  $\tilde{s}$  and  $\tilde{m}$  from the knowledge of  $B$  and  $C$  alone. This lack of information does not concern the spin (which can be exactly determined from the ratio  $B/C$ ), but only the ratio  $\tilde{m}/\sqrt{\kappa}$  (instead of the mass  $\tilde{m}$  and the parameter  $\kappa$  separately) can be determined. Using the information of tables III and V, we have calculated the ratios  $B/C$  and  $B/C^2$ , from which we have derived  $\tilde{s}$  and  $\tilde{m}/\sqrt{\kappa}$ . With SLT ( $pp/\bar{p}p$ ) we find  $\tilde{s} = 1.367(87)$ , which is not far from the spin  $\tilde{s} = 3/2$  of the  $\Omega^\pm$  baryon, and  $\tilde{m}/\sqrt{\kappa} = 0.98(21)$  GeV, which for the mass of the  $\Omega^\pm$  baryon implies  $\kappa \simeq 2.9 > 2$ , i.e., outside of the unitarity window ( $0 \leq \kappa \leq 2$ ). Instead, for SLT (all reactions) we find  $\tilde{s} = 2.33(30)$ , which is close to the spin  $\tilde{s} = 2$  of the  $2^{++}$  glueball, and  $\tilde{m}/\sqrt{\kappa} = 4.03(89)$  GeV, which for the mass of the  $2^{++}$  glueball implies  $\kappa \simeq 0.35 < 1$ , not far from the estimate that can be obtained from experimental data (see below).

(For comparison, we recall here two other theoretical predictions for the ratio  $B/C$ , obtained using completely different approaches: in Ref. [22] the value  $B/C = -1/2$  is found, which agrees with the first eq. (22) when  $\tilde{s} = 3/2$ , while in Ref. [23] the value  $B/C = -1/4$  is derived.)

We have also performed fits with  $B = B_{\text{th}}$ ,  $C = 0$  fixed ( $\text{LT}_{\text{th}}$ ) and  $B = B_{\text{th}}$ ,  $C = C_{\text{th}}$  fixed ( $\text{SLT}_{\text{th}}$ ), using for  $B_{\text{th}}$  and  $C_{\text{th}}$  the values discussed in Ref. [14] (and recalled in sec. II), corresponding to the  $\Omega^\pm$  baryon and the  $2^{++}$  and  $3^{+-}$  glueball states. In this class of variants ( $B$  and  $C$  fixed to theoretical values), the best result is  $\text{LT}_{\text{th}}$  with  $\Omega^\pm$  baryon values (both in the  $pp/\bar{p}p$  and all reactions cases).

Finally, we have also considered fits where the  $B$  and  $C$  parameters are set to  $B = \kappa B_{\text{th}}$  and  $C = \kappa C_{\text{th}}$ , with  $\kappa$  treated as an extra free parameter, which is associated to the asymptotic value of the ratio  $\sigma_{\text{el}}/\sigma_{\text{tot}}$  [eq. (16)]. In table VII we display all the resulting values together with the corresponding uncertainty (calculated via standard error propagation). The fits with the  $\Omega^\pm$  baryon values indicate an asymptotic scenario in the anti-shadowing regime, since  $\sigma_{\text{el}}/\sigma_{\text{tot}} > 0.5$ . On the other hand, the values inferred from the fits with  $B$  and  $C$  fixed to the values obtained from the  $2^{++}$  glueball state indicate a *grey-disk* scenario, with  $\sigma_{\text{el}}/\sigma_{\text{tot}} \sim 0.3$ . This value is in agreement with the asymptotic ratio obtained in other

Table VII: Ratio  $\sigma_{\text{el}}/\sigma_{\text{tot}} = \kappa/2$ , with  $\kappa$  determined from the fit LT (considering  $B = \kappa B_{\text{th}}$ , i.e.,  $\kappa = B/B_{\text{th}}$ ) and from the fit  $\text{SLT}_{\text{th},\kappa}$  to  $pp$  and  $\bar{p}p$  data only, and also from fits where all data are considered. Uncertainties are calculated with standard error propagation.

	Fits to $pp/\bar{p}p$ data only		Fits to all data	
	LT	$\text{SLT}_{\text{th},\kappa}$	LT	$\text{SLT}_{\text{th},\kappa}$
$\Omega^\pm$ baryon	0.5157(86)	0.6885(91)	0.553(10)	0.720(12)
$2^{++}$ glueball	0.2701(45)	0.3080(48)	0.2896(55)	0.3265(60)
$3^{+-}$ glueball	0.1454(24)	0.1548(26)	0.1560(29)	0.1652(32)

studies:

- empirical fits to the  $\sigma_{\text{el}}/\sigma_{\text{tot}}$  data made by Fagundes, Menon and Silva [51];
- independent fits to  $\sigma_{\text{tot}}$  and  $\sigma_{\text{el}}$  data also made by Fagundes, Menon and Silva [48, 50, 52] that yield this ratio close to 0.3;
- the prediction made by Kohara, Ferreira, and Kodama [53], using the Stochastic Vacuum Model and fits to elastic scattering data, that this ratio is below 1/2 (and close to 1/3);
- the scenario of a *black torus* proposed by Dremin [54–56], where the particle has a semi-transparent center (*grey disk*) surrounded by a *black disk*. This scenario has also been proposed, in a different context, in Refs. [57, 58].

Using the mass and spin of the  $3^{+-}$  glueball state, we also get a *grey-disk* scenario: however, the resulting asymptotic value is smaller than the experimental data available so far. From table VII, we see that the value for this ratio is around 0.15, while the experimental value at the highest energy obtained so far (8 TeV) is approximately 0.27. Since by now the data show a rising trend with energy (see for instance fig. 1 in Ref. [51]), this means that if this scenario is the correct one, then the data must present a local maximum and then decrease as the energy increases until it reaches the asymptotic value. Although there seems to be no theoretical reason to exclude this type of behavior, it seems quite unlikely to happen, and we would rather expect a smooth rise with energy until the asymptotic value is reached.

We recall that, as mentioned in section II, the result obtained in Ref. [14] also includes a subleading term  $Q^{ab} \ln s$ , where  $Q^{ab}$  is a reaction-dependent parameter. We avoided this term in the present analysis in order to study the universality of the leading ( $\ln^2 s$ ) and subleading ( $\ln s \ln \ln s$ ) terms, leaving it to future work. We also remark that the universality of  $\kappa$  is part of our assumptions.

Another important aspect to keep in mind is that  $\ln s \ln \ln s$  is a slowly varying function, so that we may need high-energy data in a larger range than what is currently available in order to be able to properly estimate the contribution of the subleading term. Therefore, new measurements of  $\sigma_{\text{tot}}$  (and also  $\sigma_{\text{el}}$ ) at 13 TeV and higher energies are fundamental to improve and confirm the results presented here.

## ACKNOWLEDGMENTS

P.V.R.G. Silva thanks the financial support by São Paulo Research Foundation (FAPESP) under the contracts 2013/27060-3 and 2015/21855-0. The authors thanks M.J. Menon for useful discussions.

- 
- [1] F. Halzen and A. D. Martin, *Quarks and Leptons: An Introductory Course in Modern Particle Physics* (Wiley, New York, USA, 1984).
  - [2] G. Pancheri and Y. N. Srivastava, arXiv:1610.10038 [hep-ph].
  - [3] M. Froissart, Phys. Rev. **123**, 1053 (1961).
  - [4] A. Martin, Phys. Rev. **129**, 1432 (1963).
  - [5] A. Martin, Nuovo Cim. A **42**, 930 (1965).
  - [6] P. D. B. Collins, *An Introduction to Regge Theory and High-Energy Physics*, Cambridge Monographs on Mathematical Physics (Cambridge Univ. Press, Cambridge, UK, 2009).
  - [7] V. Barone and E. Predazzi, *High-Energy Particle Diffraction*, Texts and Monographs in Physics, Vol. 565 (Springer-Verlag, Berlin Heidelberg, 2002).
  - [8] G. Antchev *et al.* (TOTEM Collaboration), Europhys. Lett. **96**, 21002 (2011), arXiv:1110.1395 [hep-ex].
  - [9] G. Antchev *et al.* (TOTEM Collaboration), Europhys. Lett. **101**, 21002 (2013).

- [10] G. Antchev *et al.* (TOTEM Collaboration), *Europhys. Lett.* **101**, 21004 (2013).
- [11] G. Antchev *et al.* (TOTEM Collaboration), *Phys. Rev. Lett.* **111**, 262001 (2013), arXiv:1308.6722 [hep-ex].
- [12] G. Antchev *et al.* (TOTEM Collaboration), *Eur. Phys. J.* **C76**, 661 (2016), arXiv:1610.00603 [nucl-ex].
- [13] G. Aad *et al.* (ATLAS Collaboration), *Nucl. Phys. B* **889**, 486 (2014), arXiv:1408.5778 [hep-ex].
- [14] M. Giordano and E. Meggiolaro, *JHEP* **03**, 002 (2014), arXiv:1311.3133 [hep-ph].
- [15] O. Nachtmann, *Annals Phys.* **209**, 436 (1991).
- [16] H. G. Dosch, E. Ferreira, and A. Krämer, *Phys. Rev. D* **50**, 1992 (1994), arXiv:hep-ph/9405237 [hep-ph].
- [17] M. Rueter and H. G. Dosch, *Phys. Lett. B* **380**, 177 (1996).
- [18] O. Nachtmann, *Lect. Notes Phys.* **479**, pp.1 (1997).
- [19] E. R. Berger and O. Nachtmann, *Eur. Phys. J. C* **7**, 459 (1999), arXiv:hep-ph/9808320 [hep-ph].
- [20] A. I. Shoshi, F. D. Steffen, and H. J. Pirner, *Nucl. Phys. A* **709**, 131 (2002), arXiv:hep-ph/0202012 [hep-ph].
- [21] A. Martin and S. M. Roy, *Phys. Rev. D* **89**, 045015 (2014), arXiv:1306.5210 [hep-ph].
- [22] H. Nastase and J. Sonnenschein, *Phys. Rev. D* **92**, 105028 (2015), arXiv:1504.01328 [hep-th].
- [23] V. Errasti Díez, R. M. Godbole, and A. Sinha, *Phys. Lett. B* **746**, 285 (2015), arXiv:1504.05754 [hep-ph].
- [24] E. Meggiolaro, *Z. Phys. C* **76**, 523 (1997), arXiv:hep-th/9602104 [hep-th].
- [25] E. Meggiolaro, *Eur. Phys. J. C* **4**, 101 (1998), arXiv:hep-th/9702186 [hep-th].
- [26] E. Meggiolaro, *Nucl. Phys. B* **625**, 312 (2002), arXiv:hep-ph/0110069 [hep-ph].
- [27] E. Meggiolaro, *Nucl. Phys. B* **707**, 199 (2005), arXiv:hep-ph/0407084 [hep-ph].
- [28] M. Giordano and E. Meggiolaro, *Phys. Rev.* **D74**, 016003 (2006), arXiv:hep-ph/0602143 [hep-ph].
- [29] E. Meggiolaro, *Phys. Lett.* **B651**, 177 (2007), arXiv:hep-ph/0612307 [hep-ph].
- [30] M. Giordano and E. Meggiolaro, *Phys. Lett. B* **675**, 123 (2009), arXiv:0902.4145 [hep-ph].
- [31] R. M. Corless, G. H. Gonnet, D. E. Hare, D. J. Jeffrey, and D. E. Knuth, *Adv. Comput. Math.* **5**, 329 (1996).

- [32] C. J. Morningstar and M. J. Peardon, Phys. Rev. D **60**, 034509 (1999), arXiv:hep-lat/9901004 [hep-lat].
- [33] K. A. Olive *et al.* (Particle Data Group), Chin. Phys. C **38**, 090001 (2014).
- [34] C. Patrignani *et al.* (Particle Data Group), Chin. Phys. C **40**, 100001 (2016).
- [35] M. M. Block and R. N. Cahn, Rev. Mod. Phys. **57**, 563 (1985).
- [36] S. M. Troshin and N. E. Tyurin, Phys. Lett. B **316**, 175 (1993), arXiv:hep-ph/9307250 [hep-ph].
- [37] S. M. Troshin and N. E. Tyurin, Int. J. Mod. Phys. A **22**, 4437 (2007), arXiv:hep-ph/0701241 [hep-ph].
- [38] G. Antchev *et al.* (TOTEM Collaboration), Nucl. Phys. B **899**, 527 (2015), arXiv:1503.08111 [hep-ex].
- [39] M. Aaboud *et al.* (ATLAS Collaboration), Phys. Lett. B **761**, 158 (2016), arXiv:1607.06605 [hep-ex].
- [40] J. R. Cudell, V. Ezhela, P. Gauron, K. Kang, Yu. V. Kuyanov, S. Lugovsky, B. Nicolescu, and N. Tkachenko, Phys. Rev. D **65**, 074024 (2002), arXiv:hep-ph/0107219 [hep-ph].
- [41] <http://pdg.lbl.gov/2015/hadronic-xsections/hadron.html>.
- [42] G. Aielli *et al.* (ARGO-YBJ Collaboration), Phys. Rev. D **80**, 092004 (2009), arXiv:0904.4198 [hep-ex].
- [43] P. Abreu *et al.* (Pierre Auger Observatory), Phys. Rev. Lett. **109**, 062002 (2012), arXiv:1208.1520 [hep-ex].
- [44] R. U. Abbasi *et al.* (Telescope Array), Phys. Rev. **D92**, 032007 (2015), arXiv:1505.01860 [astro-ph.HE].
- [45] F. James, *MINUIT Function Minimization and Error Analysis: Reference Manual Version 94.1* (1994).
- [46] P. Bevington and D. Robinson, *Data Reduction and Error Analysis for the Physical Sciences Boston* (McGraw-Hill, Massachusetts, 1992).
- [47] <http://root.cern.ch/>.
- [48] M. J. Menon and P. V. R. G. Silva, J. Phys. G **40**, 125001 (2013), [Erratum: J. Phys. G **41**, 019501(2014)], arXiv:1305.2947 [hep-ph].
- [49] M. M. Block and F. Halzen, Phys. Rev. D **73**, 054022 (2006), arXiv:hep-ph/0510238 [hep-ph].
- [50] M. J. Menon and P. V. R. G. Silva, Int. J. Mod. Phys. A **28**, 1350099 (2013), arXiv:1212.5096

- [hep-ph].
- [51] D. A. Fagundes, M. J. Menon, and P. V. R. G. Silva, Nucl. Phys. A **946**, 194 (2016), arXiv:1509.04108 [hep-ph].
- [52] D. A. Fagundes, M. J. Menon, and P. V. R. G. Silva, J. Phys. G **40**, 065005 (2013), arXiv:1208.3456 [hep-ph].
- [53] A. K. Kohara, E. Ferreira, and T. Kodama, Eur. Phys. J. C **74**, 3175 (2014), arXiv:1408.1599 [hep-ph].
- [54] I. M. Dremin, JETP Lett. **99**, 243 (2014), arXiv:1401.3106 [hep-ph].
- [55] I. M. Dremin, Bull. Lebedev Phys. Inst. **42**, 21 (2015), [Kratk. Soobshch. Fiz.42,no.1,8(2015)], arXiv:1404.4142 [hep-ph].
- [56] I. M. Dremin, Phys. Usp. **58**, 61 (2015), arXiv:1406.2153 [hep-ph].
- [57] P. Desgrolard, L. L. Jenkovszky, and B. Struminsky, Eur. Phys. J. C **11**, 145 (1999).
- [58] P. Desgrolard, L. L. Jenkovszky, and B. V. Struminsky, Phys. Atom. Nucl. **63**, 891 (2000), [Yad. Fiz. 63, 962 (2000)].